Advanced Multiresponsive Comploids: From Design to Possible Applications

Jérôme J. Crassous,*[a,b] Adriana M. Mihut,[a,b] Hervé Dietsch, [b‡] Olivier Pravaz,[b] Liliane Ackermann-Hirschi,[b] Ann M. Hirt,[c] and Peter Schurtenberger[a]

Dynamic Light Scattering (DLS) characterization of the silica-coated spindle-type particles

The translational diffusion coefficients D_T of the silica-coated hematite (SCHs) and silica-coated maghemite (SCMs) particles were determined by dynamic light scattering. Hereby the decay rate Γ of the correlation function measured at different scattering angles, θ, provides D_T through $\Gamma = q^2 D_T$, with the magnitude of the scattering vector q given by $q = 4\pi n sin(\theta/2)/\lambda_0$, where n is the refractive index of the solvent and λ_0 is the wavelength of the incident beam. For prolate ellipsoids, one can estimate D_T using:[1,2]

$$D_T = \frac{k_B T G(\rho)}{3\pi\eta a_{SCH}} \quad (1)$$

where $G(\rho)$ corresponds to

$$G(\rho) = (1-\rho^{-2})^{-\frac{1}{2}} ln\left(\rho\left(1+(1-\rho^{-2})^{-\frac{1}{2}}\right)\right) \quad (2)$$

where a_{SCH} refers to the long axis of the coated hematite and ρ to its aspect ratio. Following the approach described in recent studies on similar particles,[2,3] D_T was estimated from the statistics of TEM pictures over 100 analyzed particles shown in Fig. S1. As the scattered intensity is proportional to the square of the volume of a single particle, the corresponding weighting follows:

$$D_{T,t_h} = \frac{\sum(D_i V_i^2)}{\sum(V_i^2)} \quad (3)$$

where D_i and V_i are the translational diffusion coefficient and volume of each single particle in the data set, respectively.

[a] *Physical Chemistry, Department of Chemistry, Lund University, 22100 Lund, Sweden. E-mail:jerome.crassous@fkem1.lu.se*
[b] *Adolphe Merkle Institute, University of Fribourg, 1723 Marly, Switzerland.*
[c] *Institute for Geophysics, ETH Zürich, 8092 Zürich, Switzerland.*
‡ Present address: BASF SE, Modelling and Formulation Research, Formulation Platform, 67056 Ludwisghafen am Rhein, Germany.

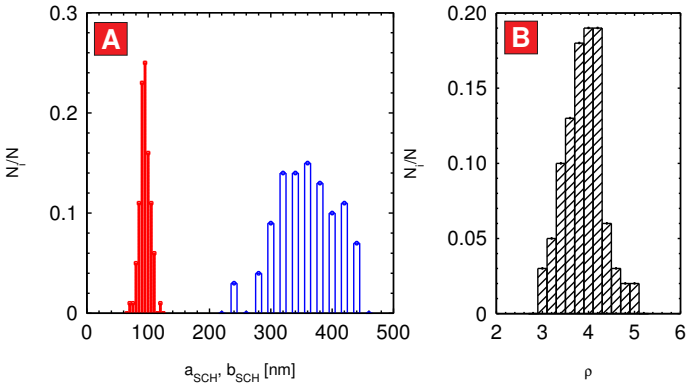

Fig. S 1 Statistical distribution of the silica coated long and short axis, a_{SCH} and b_{SCH} (A) and aspect ratio ρ (B).

Magnetic properties of the silica-coated spindle-type particles

The magnetic properties were estimated from the magnetization, M, measured as a function of the applied field, H, on a vibrating sample magnetometer (VSM) (see Fig. 2D). The dependence between M and H could be well described with the Langevin equation following:

$$M = \sigma_S\left(coth\frac{\mu_0\mu H}{k_B T} - \frac{k_B T}{\mu_0\mu H}\right) + \chi_{HF} H \quad (4)$$

where σ_S is the saturation magnetization, μ_0 is the magnetic constant, μ is the magnetic moment of the particle and χ_{HF} is the high field susceptibility. σ_S and χ_{HF} were estimated from the asymptotic behavior at high magnetic fields with VSM, and the magnetic susceptibility, χ, was independently determined on a Kappabridge. σ_S, χ_{HF} and χ were measured at $1.69.10^{-1}$ Am^2/kg, $3.02.10^{-7}$ m^3/kg and $1.26.10^{-6}$ m^3/kg, *i.e.*, for the pure hematite particles in good agreement with literature values.[4,5] After coating, the measured σ_S and χ_{HF} decrease to $7.27.10^{-2}$ Am^2/kg and $9.19.10^{-8}$ m^3/kg, respectively. This can be related to the mass fraction of hematite in the particles. Hereby, the ratio of σ_S after and before coating equals to 0.43. Considering the dimensions from the TEM analysis and a density for the hematite of 5.26 g/cm^3, and for the silica shell of 2.06 g/cm^3,[5] the mass fraction of hematite

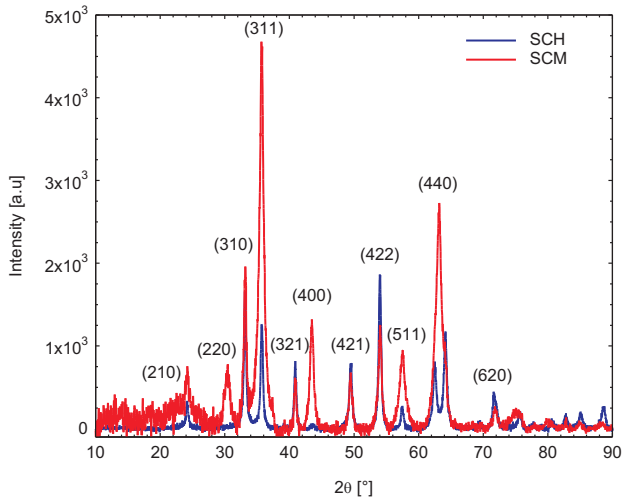

Fig. S 2 XRD patterns refined by the Rietveld method corresponding to SCH and SCM nanoparticle powders. SCM particles have a hybrid composition consisting of 70 wt% γ-Fe_2O_3 (maghemite) and 30 wt% α-Fe_2O_3 (hematite) determined from the Retveld refinement.

could be estimated to 0.53. This analysis clearly overestimates this fraction as it neglects the porosity of the hematite core estimated at 26 vol% on a similar system.[6] Assuming that the pores are filled with silica, we obtained a value of 0.43 for the hematite mass fraction. The measurement of σ_S is therefore in good agreement with the composition of the particles. The same approach could be applied to the ratio of χ_{HF} equal to 0.3. The lower ratio could be due to the fact that the silica may isolate the magnetic domains, which will have direct consequences on the susceptibility of the materials.[6] This is what is observed in our materials as the measured coercivity H_C decreases from 26.0 to 1.0 kA/m after coating, in contrast to the susceptibility, which increases from $1.26.10^{-6}$ to $3.98.10^{-6}$ m^3/kg. After their partial transformation into maghemite, the particles exhibit a strong increase of σ_S by a factor 81 to 5.91 Am^2/kg and χ by a factor 77 to $3.05.10^{-4}m^3$/kg. The measured coercivity then increases by a factor 2.1 to 2.1 kA/m. Hereby, if χ is compatible with the value reported in the literature,[4] σ_S is almost three times lower than the expecterd value from maghemite. This low value may be due to the presence of hematite or to magnetic interaction between the particles.

XRD investigation of the hematite transformation into maghemite

The XRD patterns of SCH and SCM particles are shown in Fig. S2. The diffraction pattern of SCM clearly differs from that of the initial SCH, indicating that the crystalline phase of iron oxide changed from α-Fe_2O_3 to γ-Fe_2O_3. Extra reflection lines from maghemite were evident on the patterns, whereas the reflection lines from the original hematite were absent from the pattern, indicating that the original SCH was mostly converted to SCM. Rietveld refinement of XRD patterns obtained from reduced powders is used to determine the crystalline phases of iron oxide particles. Rietveld refinement was made using the TOPAS3 software package (Bruker Inc.). The refined structural parameters are the lattice parameters, atomic positions, isotropic temperature coefficients, single scattering column height, strain and preferred orientation. For the analysis of SCM we used the space group $P4_332$ and the lattice constant for this cubic structure was found to be $a = 8.342$ Å, whereas SCH had a corundum-type crystal structure refine in rhombohedral $R\bar{3}c$ space group. We evaluate a conversion to a final state with 70% γ-Fe_2O_3 and 30% α-Fe_2O_3.

Cryogenic electron microscopy (cryo-TEM) investigation of the hybrid microgels

The hybrid microgels were imaged by cryo-TEM as shown in Fig. S3. The dilute suspensions were maintained at room temperature and then rapidly vitrified, in such a way that the conformation in suspension is mostly preserved as shown in former studies on composite microgels.[7–9] The analysis of the PNIPMAM/SCM microgels (Fig. S3 A, B) confirms that all the particles are embedded within a crosslinked microgel network and that the core of most particles consists of a single SCM. The two hybrid microgels loaded with AuNPs (Fig. S3 C-F) are homogeneously decorated. When comparing the AuNP distribution within these two hybrids, AuNPs/PNIPMAM/SCM particles were found to bear a larger amount of AuNPS than PNIPAM/AuNPs/PNIPMAM/SCM particles, which are partially free as the consequence of the fast vitrification process. This shows that some of the particles may not be strongly absorbed within the microgels. This is supported by the finding that after the synthesis of the additional PNIPAM network and the subsequent purification process, the hybrid contains less AuNPs. Nevertheless, these last ones are strongly attached to the particles as confirmed by the very low amount of free AuNPs. Further on, the microgel shell surrounding the particles appears much denser and the overall shape is more anisotropic. This is a clear and direct evidence of the so-called ”corset” effect proposed by scattering studies on PNIPAM/PNIPMAM microgel systems.[10,11]

Distribution of AuNPs in the AuNPs/PNIPMAM/SCM

Fig. S4 shows a larger magnification of the lateral cross-section of the hybrid particle after reduction of AuNPs. The AuNPs are uniformly distributed within the shell and have an

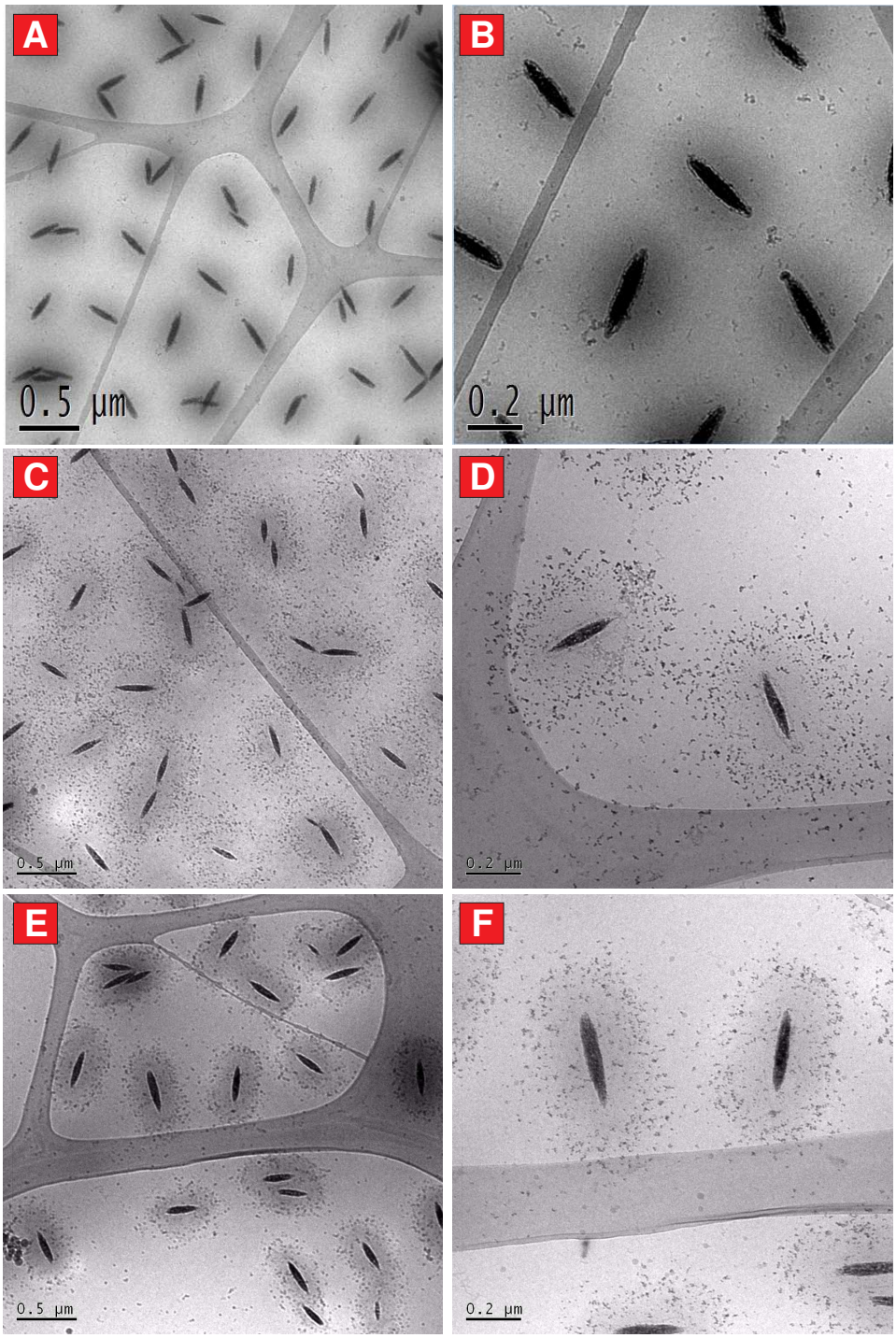

Fig. S 3 Cryogenic transmission electron microscopy of the hybrid microgels: A, B) PNIPMAM/SCM particles, C, D) AuNPs/PNIPMAM/SCM particles, E, F) PNIPAM/AuNPs/PNIPMAM/SCM particles.

average radius of 1.4 ± 0.6 nm. A former study of the loading of anionic microgels with anionic gold nanoparticles with different sizes has demonstrated that the physical entrapment of AuNPs within the microgels is suppressed when the AuNP size is of the order of the microgel mesh size or larger.[12] For this reason we consider that the mesh size of the microgels

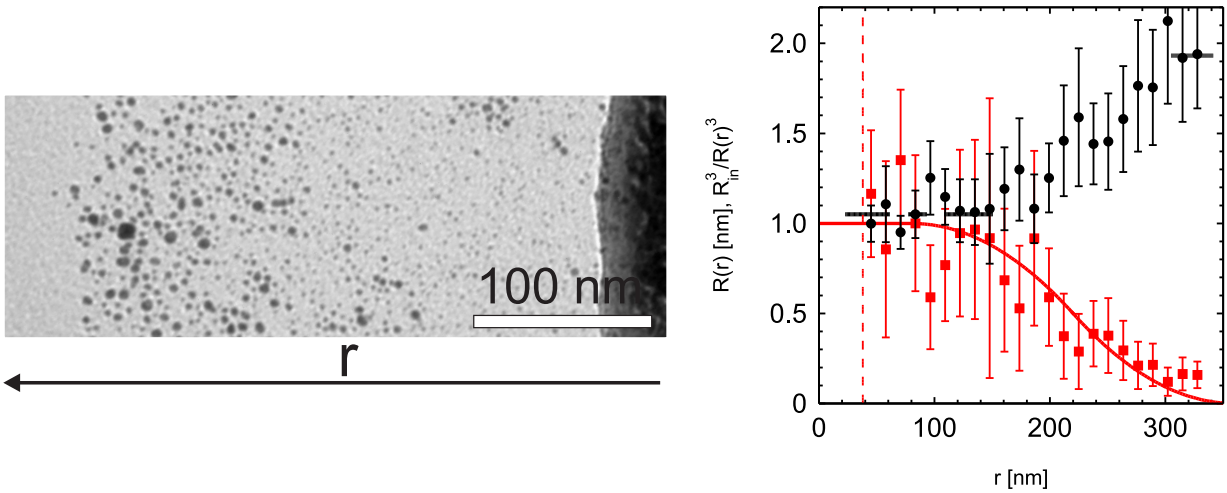

Fig. S 4 Transversal size distribution of the average gold nanoparticles of AuNPs/PNIPMAM/SCM hybrid microgels. Circles refer to the average AuNPs radius $R(r)$, and squares to the estimation of the normalized polymer density profile $\phi_r(r) = R_{in}^3/R(r)^3$ fitted with equation 6 (see text for further explanation).

can be related to the growth of the particles. This is motivated by our estimation of the average mesh size, ξ, which is calculated from the mass of a SCM, m_{SCM}, approximated from its average dimensions and the density of the magnetic core (30 wt% α-Fe_2O_3, ρ_H = 5.26 g.cm^{-3} and 70 wt% γ-Fe_2O_3, ρ_M = 4.90 g.cm^{-3}) and silica shell (ρ_S = 2.06 g.cm^{-3}), the mass ratio between the BIS crosslinker and the SCM, α, determined from the synthesis of the PNIPMAM/SCM, and the overall size of the PNIPMAM/SCM hybrid microgels given by their hydrodynamic radius measured at 20^{o}C:

$$\xi = \left(\frac{4\pi M_{BIS} \left(R_H^3 - a_{SCH} b_{SCH}^2/8 \right)}{3 N_A \alpha m_{SCM}} \right)^{\frac{1}{3}} \qquad (5)$$

Such a calculation leads to an average mesh size in the order of 3 to 4 nm compatible with the average diameter of the AuNPs. Nevertheless, the density profile of a microgel is not homogeneous, but gradually decays at the surface as an error function[13] following:

$$\phi_r(r) = \begin{cases} 1 & : \quad r \leq R_c \\ 1 - (R_{hw} - r - 2\sigma)^2/(8\sigma^2) & : \quad R_c < r \leq R_{hw} \\ (r - R_{hw} - 2\sigma)^2/(8\sigma^2) & : \quad R_{hw} < r < R_t \\ 0 & : \quad R_t \leq r \end{cases} \qquad (6)$$

where $\phi_r(r)$ is the density profile $\phi(r)$ normalized by the plateau value close to the core ϕ_c. R_c refers to the radius of the core and R_{hw} to the half-width radius such as $R_{hw} = R_c + 2\sigma$, with σ corresponding to the half-width. R_t is the total radius and is defined as $R_t = R_{hw} + 2\sigma$. As a direct consequence, the radius of the AuNPs increases with the distance from the center to the periphery from about 1 to 2 nm. If we now consider that the volume of the particles is inversely related to the polymer volume fraction $\phi(r)$, the normalized polymer density profile $\phi_r(r)$ could then be estimated as $R_{in}^3/R(r)^3$, where R_{in} is the radius of the particles close to the silica surface. The following profile in Fig. S4 was then described using equation 6 with R_{hw} = 220 nm and σ = 70 nm. This simple approach confirms that, in our case, the particles distributed within the microgel adapt to the mesh size of the polymeric matrix.

Temperature-induced coagulation

We follow the effect of temperature on the particle stability by time resolved aggregation experiments performed on a 3D DLS instrument in cross-correlation mode. A dilute suspension of PNIPAM/AuNPs/ PNIPMAM/SCM particles (1.10^{-3} gL^{-1}) containing 0.1 M KCl was quenched at different temperatures following the protocol established in a former study.[14] The temporal evolution of the apparent hydrodynamic radius R_H determined from a second order cumulant analysis was measured for about 1 hour. Below 40^{o}C, the particles are stable, with an R_H value about 30 nm lower than without the addition of salt as observed in others studies on microgels.[15,16] Above 40^{o}C, the particles first equilibrate at a R_H value of about 150 nm independent on the temperature and then become unstable. The data shown in Fig. S5A were normalized by $R_{H,1}$, that is, the hydrodynamic radius before the onset of the aggregation process, and the time was rescaled to the onset of the aggregation. This analysis shows that the aggregation rate increases at higher temperatures, which is related to the combined contributions of the increase of the at-

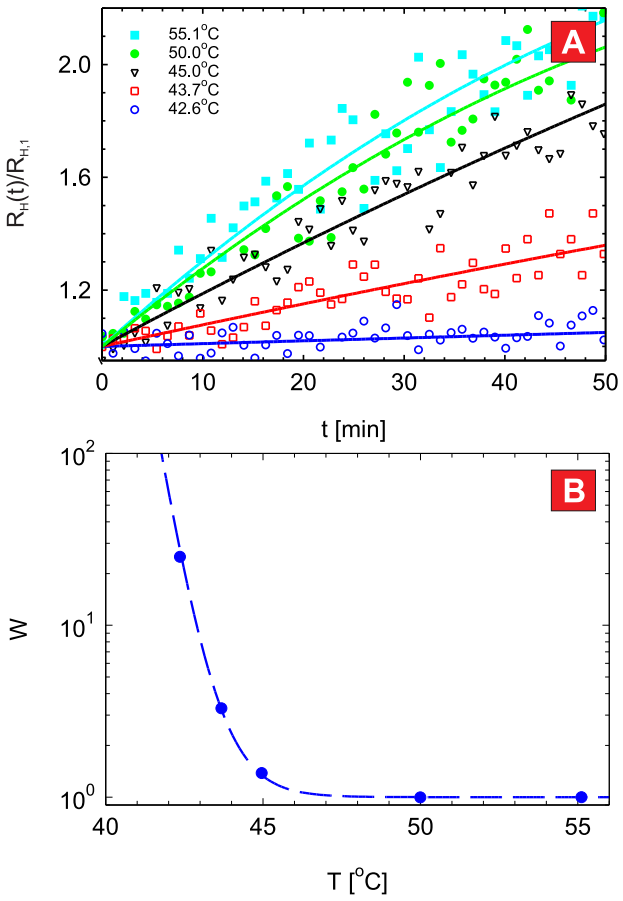

Fig. S 5 A) Time evolution of the normalized hydrodynamic radius of a dilute PNIPAM/AuNPs/PNIPMAM/SCM suspension (c = 1.10^{-3} gL^{-1}) quenched to different temperatures. B) Evaluation of the corresponding stability ratio, W, fitted from equation 9 (dashed line).

traction forces and to the decrease of the solvent viscosity. In order to quantify the stability of the particles, we first determined the aggregation rate constants $k_{agg}(T)$ at the different temperatures from the initial slope of $R_H(t)/R_{H,1}$ obtained from a second order polynomial fit. In the diffusion limited aggregation regime, both η and T contribute to the aggregation kinetics as suggested by the Smoluchovski expression, where k_{agg} in the diffusion limited regime is equal to $8k_BT/\eta$. For this reason, we define a relative stability ratio, W, that takes into account the effect of both viscosity and temperature following:

$$W = \frac{T_{fast}}{T} \cdot \frac{\eta(T)}{\eta(T_{fast})} \cdot \frac{k_{agg}(T_{fast})}{k_{agg}(T)} \qquad (7)$$

where the fast aggregation rate $k_{agg}(T_{fast})$ was considered at T_{fast} = 328.16 K. As shown in Fig. S5 B, W first sharply decreases from 42 to 45^oC in the vicinity of the volume phase transition temperature and reaches a constant value above 45^oC. Following a recent approach proposed for the aggregation of PS/PNIPAM composite microgels,[14] we can interprete this result by considering a two-level system that is either hydrophilic or hydrophobic, where the probability distribution of the hydrophobic particles p_B can be expressed as:

$$p_B = exp\,(-(T_c - T)\Delta S/k_BT)^{-1} \qquad (8)$$

in which ΔS characterizes the change of entropy between the two states, and where T_c is the transition temperature. In the early stage of the aggregation the probability to form a doublet can be approximated by p_B^2. Assuming that the particles interact through a square well potential with a minimum $V_{min}(T)$, W can be estimated as follows:

$$\frac{V_{min}(T_{fast})}{V_{min}(T)} = (1 + exp(-(T_c - T)\Delta S/k_BT))^2 \approx W \qquad (9)$$

This model provides a good description of the experimental data for T_c = 43.5+273.16 K and ΔS = -400k_B. In comparison to PS/PNIPAM composite microgels where T_c = 32+273.16 K and ΔS = -1420k_B,[14] T_c shifts to a higher temperature corresponding to the volume phase transition temperature of the hybrid microgel, and ΔS is of the same order but lower, probably due to the interwoven PNIPAM and PNIPMAM networks in the shell.

References

1 F. Perrin, *J. Phys. Radium VII*, 1934, **5**, 497–511.
2 I. Martchenko, H. Dietsch, C. Moitzi and P. Schurtenberger, *J. Phys. Chem. B*, 2011, **115**, 14838–14845.
3 A. M. Mihut, A. Sanchez-Ferrer, J. J. Crassous, L. A. Hirschi, R. Mezzenga and H. Dietsch, *Polymer*, 2013, **54**, 4194–4203.
4 C. Peters and M. J. Dekkers, *Phys. Cem. Earth*, 2003, **28**, 659–667.
5 M. Reufer, H. Dietsch, U. Gasser, A. M. Hirt, A. Menzel and P. Schurtenberger, *J. Phys. Chem. B*, 2010, **114**, 4763–4769.
6 M. Reufer, H. Dietsch, U. Gasser, B. Grobety, A. M. Hirt, V. K. Malik and P. Schurtenberger, *J. Phys. Condens. Mat.*, 2011, **23**, 065102.
7 J. J. Crassous, M. Ballauff, M. Drechsler, J. Schmidt and Y. Talmon, *Langmuir*, 2006, **22**, 2403–2406.
8 Y. Lu, Y. Mei, M. Drechsler and M. Ballauff, *J. Phys. Chem. B*, 2006, **110**, 3930–3937.
9 J. J. Crassous, C. N. Rochette, A. Wittemann, M. Schrinner and M. Ballauff, *Langmuir*, 2009, **25**, 7862–7871.
10 I. Berndt and W. Richtering, *Macromolecules*, 2003, **36**, 8780–8785.
11 I. Berndt, J. S. Pedersen and W. Richtering, *Angew. Chem. Int. Ed.*, 2006, **45**, 1737–1741.
12 M. Kuang, D. Y. Wang and H. Mhwald, *Adv. Funct. Mater.*, 2005, **15**, 1611–1616.
13 M. Stieger, J. Pedersen, P. Lindner and W. Richtering, *J. Chem. Phys.*, 2004, **120**, 6197.
14 A. Zaccone, J. J. Crassous, B. Béri and M. Ballauff, *Phys. Rev. Lett.*, 2011, **107**, 168303.
15 T. López-Léon, J. L. Ortega-Vinuesa, D. Bastos-Gonzalez and A. Elaïssari, *J. Phys. Chem. B*, 2006, **110**, 4629–4636.
16 B. Tan, R. Pelton and K. Tam, *Polymer*, 2010, **51**, 3238–3243.